Entanglements in P3HT and Their Influence on Thin-Film Mechanical Properties: Insights from Molecular Dynamics Simulations

Naga Rajesh Tummala,[1] Chad Risko,[1,2] Christopher Bruner,[3] Reinhold H. Dauskardt,[3] Jean-Luc Brédas[1,4]

[1]School of Chemistry and Biochemistry and Center for Organic Photonics and Electronics, Georgia Institute of Technology, Atlanta, Georgia 30332-0400
[2]Department of Chemistry and Center for Applied Energy Research, University of Kentucky, Lexington, Kentucky 40506-0055
[3]Department of Materials Science and Engineering, Stanford University, Palo Alto, California 94305-4034
[4]Solar and Photovoltaics Engineering Research Center, King Abdullah University of Science and Technology, Thuwal 23955-6900, Kingdom of Saudi Arabia
Correspondence to: C. Risko (E-mail: chad.risko@uky.edu) or J.-L. Brédas (E-mail: jean-luc.bredas@kaust.edu.sa)

Received 0 Month 2014; revised 0 Month 2015; accepted 0 Month 2015; published online 00 Month 2015
DOI: 10.1002/polb.23722

ABSTRACT: Due to their inherent mechanical flexibility and stretchability, organic-based electronic devices have garnered a great deal of academic and industrial interest. Here, molecular-dynamics simulations are used to examine the molecular-scale details that govern the relationships among molecular weight, chain entanglement, persistence length, and the elastic characteristics of the widely studied π-conjugated polymer poly-(3-hexyl thiophene), P3HT. Oligomers containing at least 50 monomer units are required in the simulations to observe elastic behavior in P3HT, while much longer chains are required to ensure description of appropriate levels of entanglement: only when the molecular weight is greater than 50 kDa, that is, oligomers with approximately 400 monomer units, is truly entangled behavior observed. Interestingly, results from primitive path analysis of amorphous P3HT matches well with the observed onsets of inter-chain excitonic coherence with increased molecular weight. The simulations also indicate that the P3HT modulus saturates at 1.6 GPa for chain lengths of 50–100 monomers, a result that compares well with experimental results. This work highlights the care that needs to be taken to accurately model P3HT morphologies in relation to experimental measurements. © 2015 The Authors. Journal of Polymer Science Part B: Polymer Physics Published by Wiley Periodicals, Inc. J. Polym. Sci., Part B: Polym. Phys. **2015**, *00*, 000–000

KEYWORDS: cohesion energy; conjugated polymers; mechanical properties; molecular dynamics; polymer entanglement; P3HT

INTRODUCTION The use of semiconducting polymers has grown enormously over the last three decades.[1] Polymer-based electrically active materials can be tuned to respond to various optical, electronic, or other physical stimuli by synthetically varying the conjugated monomers.[2,3] In many emerging applications such as electronic skin, organic transistors, or solar cells, the flexibility and mechanical strength of these polymer materials represent crucial physical properties that will at least in part determine the success of future commercialization strategies.[2,4]

Regioregular poly(3-alkylthiophenes) were synthesized nearly two decades ago[5] and have served as benchmark polymers for organic electronics research,[6] from both experimental[7] and theoretical perspectives.[8–13] Among these derivatives, poly(3-hexylthiophene), P3HT, is the primary workhorse. Studies concerning the impact of regioregularity, alkyl side-chain length, and molecular weight (M_w) on the morphological properties of pure and blended polythiophene thin films[13–21] reveal that: (i) regioregularity plays an essential morphological role; (ii) the alkyl side-chains affect solubility and packing[22]; and (iii) the polymer chain M_w directly affects the thin-film material (opto)electronic properties. Many questions, however, remain to be resolved for these, and other, conjugated-polymer-based materials.

Among the growing investigations is how the sequence along conjugated polymer chains and their solid-state packing influence the mechanical properties of polymer-based (opto)electronic materials. Such considerations are important when

TABLE 1 P3HT Oligomer Sizes, Molecular Weights, Number of Chains, Total Particles in the Simulation Box, and Respective Final Simulation Box Sizes Used in the MD Simulations

P3HT Oligomer	P3HT M_w (kDa)	Number of Chains	Number of Particles	Final Box Dimensions (nm)
12-mer	2.0	60	18,120	5.75 × 5.75 × 5.75
18-mer	3.0	48	21,696	6.11 × 6.11 × 6.11
24-mer	4.0	48	28,896	6.72 × 6.72 × 6.72
50-mer	8.3	48	60,096	8.59 × 8.59 × 8.59
100-mer	16.6	24	60,048	8.59 × 8.59 × 8.59
200-mer	33.2	24	120,048	10.80 × 10.80 × 10.80
400-mer	66.5	24	240,048	13.61 × 13.61 × 13.61

contemplating manufacturing protocols and material reliability. For instance, there is a significant M_w dependence of the polymer active-layer cohesion and flexibility, properties of particular relevance for stretchable/flexible applications[23–29] as well as for organic solar-cell applications with active layers that incorporate P3HT[24] or other conjugated polymers.[25,30–34]

Using all-atom molecular-dynamics (MD) simulations, here, we seek to quantify at the moleulcar scale the entanglement and cohesive properties of P3HT as a function of M_w (chain length). The stress-strain response of bulk P3HT, with oligomer lengths ranging from 12 (2 kDa) to 400 (67 kDa) monomers, is evaluated and compared to experimental data. We show the necessity to consider long P3HT oligomer chains—lengths that are considerably longer than those commonly reported for simulations of P3HT—to accurately represent many of the key features of these polymer-based materials.

COMPUTATIONAL METHODOLOGY

The Large-Scale Atomic/Molecular Massively Parallel Simulator (LAMMPS) software suite was used for the MD simulations.[35] The modified OPLS-AA (Optimized Potentials for Liquid Simulations-All Atom)[36] force field described by Huang and co-workers[11,37] with improper angles for the intra-monomer rigidity was used, as the unmodified potential produced unphysical thiophene conformations.[8] We note that the energetic barrier to rotation of the inter-thiophene S-C-C-S dihedral angle controls the regioregularity and the rigidity of the P3HT backbone.

Simulations were carried out with oligomer lengths, N, consisting of 12, 18, 24, 50, 100, 200, and 400 monomers (Table 1). 24 ($N = 100$, 200, and 400), 48 ($N = 18$, 24, and 50), or 60 ($N = 12$) regioregular oligomers were randomly distributed in periodic simulation boxes with densities less than 0.1 gm/cc. Energy minimization followed. The energy minimized structures were then annealed for at least 1 ns using a canonical ensemble (NVT) at 800 K and 1 ns at 550 K. This was followed by an isothermal-isobaric (NPT) ensemble at 550 K and 1 atm for at least 5 ns ($>$ 10 ns for 400-mer). Final configurations were then integrated within NPT ensembles at 300 K until the total volumes and potential energies equilibrated (at least 5 ns), and then allowed to equilibrate for an additional 2 ns. In some cases, the simulations were performed at increased temperature (550 K) starting from the equilibrated configurations at 300 K, and the abovementioned procedure was implemented twice more. The resulting structural and thermodynamic properties are compared to known experimental data to validate the simulation protocol.

Temperature was kept constant during the simulations using the Nosé–Hoover thermostat with a relaxation time constant of 100 fs. The internal pressure was maintained using the Nosé–Hoover barostat as implemented in the LAMMPS software package[38,39] with the damping parameter set to 500 fs. The atomic coordinates were stored at 20–50 ps intervals depending on the system size, while thermodynamic parameters (bond, angle, dihedral, van der Waals energy, electrostatic interactions) were stored every 0.5 ps. The results reported here are computed from averaging the last 2 ns of collected data.

To compute the P3HT modulus, a series of 500 ps simulations were performed with strain increments < 0.005 %; the z-component of the stress tensor was selected to compute the uni-axial tensile (elongation) modulus. The average stress of the final 250 ps was taken as the equilibrated stress at each elongation. The slope of the equilibrated stress versus strain plot in the linear regime (less than 5% strain) is reported as the modulus. Identical methods were used for the final configurations of P3HT oligomers (12-mer to 100-mer) from simulations at 300 K to compute the uni-axial tensile modulus. These calculations were repeated at least three times and the deviation of the values is reported as error bars. Diffusion is not reported as P3HT is a viscoelastic solid with a glass transition temperature of 283 K[40,41]; dynamical properties and viscosities, which in general require larger number of chains and more strict criteria in terms of simulation box sizes, are also not reported. The modulus of the 200-mer and 400-mer P3HT were not computed as the modulus converged for the 100-mer system, and recent experiments suggest that the storage modulus is not significantly affected by M_w.[24] Stress vs. strain curves (by elongating the simulation box in z-dimension at constant strain rate of 0.01 nm/ps rather than incremental strains as mentioned earlier) were computed for oligomers of different

chain lengths to understand the elastic behavior of the oligomer chains as a function of deformation. The deformation simulations were performed with the SLLOD nonequilibrium MD equations of motion as implemented in LAMMPS.[35,42]

RESULTS AND DISCUSSION

We begin by discussing the P3HT rigidity and bulk structural and packing parameters as a function of M_w. The rigidity and planarity of P3HT are characterized by probability distributions for (i) the angle between the centers-of-mass of three consecutive thiophene units and (ii) the inter-thiophene, S—C—C—S, dihedral angle (Fig. 1). The angle along the chain is centered around 20°, indicating a very slight curve in the chain. The inter-thiophene dihedral angle peaks at 180° with a smaller dihedral peak at 20 to 25°. The relaxation of the P3HT bulk at high temperatures (550 K) does allow for rotation of the inter-monomer dihedral angle, and the small angle peak is indicative of *syn* thiophene–thiophene configurations present in our simulations. These results reveal that the P3HT backbones coming from the simulations are fairly planar with a P3HT regioregularity of ~90%.

The radial distribution functions (RDFs, Fig. 1) for P3HT 12-mers reproduce those reported by Do and co-workers,[11] while the RDFs of the 100-mer are consistent with other literature data.[11,37] The results show that modified dihedral parameters (Fig. 1), apart from keeping the backbone more rigid, do not change the description of the bulk polymer packing. From the first peak (at 5 Å) of the Site-1−Site-1 RDF (Site-1 represents center-of-mass of thiophene, see Fig. 1 for definition), it is evident that the thiophene backbones do not stack on top of each other and that there is no crystallinity arising from the simulations. Hence, the simulations reported here represent the amorphous regions of the semicrystalline polymer. We note that, owing to the random character of the starting configurations, along with the absence of explicit π-π interactions due to the isotropic nature of the thiophene–thiophene interactions in the force field, it would be difficult to observe the formation of a crystalline phase, especially with such large molecular-weight polymers (*e.g.*, for oligomers with more than 100 monomers)[43] unless Monte Carlo methods[43] or emerging rare-event sampling techniques are used.[43] The RDFs for P3HT do not change with M_w, indicating that the molecular packing in amorphous P3HT is hardly dependent on M_w.

The calculated P3HT density varies modestly with oligomer size, ranging from 1.043 to 1.053 g/cc. These values are comparable to the experimental value of 1.1 ± 0.05 g/cc for crystalline P3HT.[44,45] The minor density variations are due to differences in contributions of the end and non-end groups, which are related exponentially and linearly, respectively, to the inverse of M_w.[46]

The computed solubility parameters, although within the noise of the simulations, decrease with increasing P3HT M_w

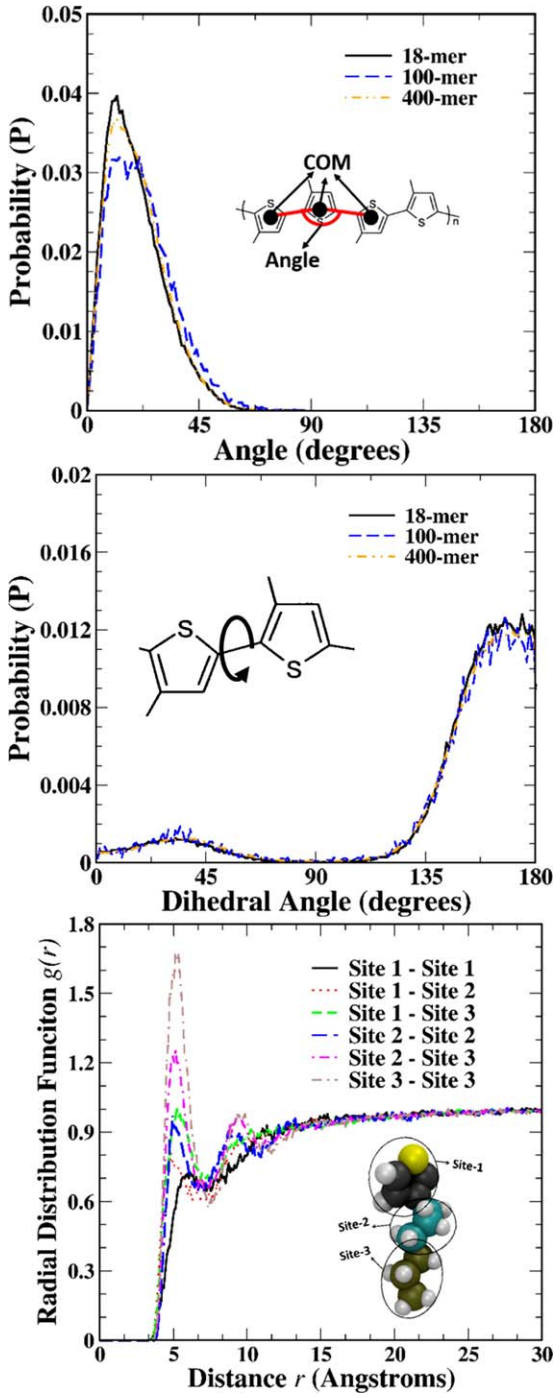

FIGURE 1 (top) Probability distribution of the angle between the centers-of-mass of three consecutive thiophene units. Cartoon in the inset showing the definition of the angle. (middle) Probability distribution of the (S-C-C-S) inter-thiophene dihedral angles (shown in the inset). (bottom) Radial distribution functions (RDFs) among the component centers-of-mass (COM) defined in the inset. Site-1 is the COM of the thiophene ring, Site-2 is the COM for the propyl moiety closest to the thiophene, and Site-3 is the COM for the propyl moiety farthest from the thiophene ring. [Color figure can be viewed in the online issue, which is available at wileyonlinelibrary.com.]

TABLE 2 Density and Hildebrand Parameters for P3HT Oligomers with Varying Chain Lengths

		δT (cal/cc)1/2	
P3HT Oligomer	Density (gm/cc) (±0.003)	Simulation (±0.05)	Experiment
12-mer	1.053	9.28	N/A
18-mer	1.043	9.25	N/A
24-mer	1.046	9.23	N/A
50-mer	1.044	9.18	N/A
100-mer	1.043	9.18	N/A
200-mer	1.046	9.21	N/A
400-mer	1.047	9.22	9.76[49]

up to the 100-mer and then increase, a feature observed in other polymer simulations.[47] We believe that the combination of density variations and excluded volume effects, influenced by the number of entanglements and entanglement length of P3HT, results in the Hildebrand parameter trends. Across the oligomer series, the calculated Hildebrand solubility parameters[48] (Table 2) are consistently smaller than the experimental value by some 0.5 $(cal/cc)^{0.5}$. The contribution of the dihedral angles to the total energy in the P3HT oligomers is absent in the monomers, resulting in lower estimates of the solubility parameters. Each of the four dihedral angles contributes roughly 0.5 kcal (from 1-4 electrostatic and dispersion interactions), yielding a solubility parameter of 9.7 to 9.8 $(cal/cc)^{0.5}$ for all the oligomers studied here. The Hansen parameter for the dispersion contribution is 8.71 $(cal/cc)^{5}$ and the combined polar hydrogen-bond contribution is 3 $(cal/cc)^{0.5}$, which is comparable to the experimental value of 9.02 and 3.67 $(cal/cc)^{0.5}$, respectively.[49] These results confirm that the OPLS-AA force-field parameters can be used to obtain reliable cohesive strengths for P3HT.

Next, we turn our attention to the polymeric and entanglement properties of P3HT as a function of M_w computed via the Z1 software package,[50–53] which computes the topological constraints on the chains using the shortest connected paths from MD trajectories. We also determined properties such as the end-to-end $<R_{ee}>$ distances, modified and classical entanglement chain lengths (N_e) based on kinks and coils, and primitive path contour length (L_{pp}). The P3HT radius of gyration (R_G) was evaluated using standard definition. Both $<R_{ee}^2>$ and $<R_G^2>$ and their ratio were calculated and are plotted in Figure 2.[54] A slight discontinuity in $<R_{ee}^2>$ and $<R_G^2>$ versus oligomer chain length (N) is observed between the 50-mer and 100-mer. Although such discontinuities are rarely noted, this is an indication of changes in P3HT chain conformation. For oligomers > 100-mer, the ratio of $<R_{ee}^2>$ and $<R_G^2>$ oscillates around 6.5, indicating convergence. However, at extremely large N (very high M_w P3HT > 100 kDa), that is, at the asymptotic limit of $N \rightarrow \infty$ the ratio should be equal to 6.[52] Larger coarse-grained simulations to study the accurate dynamics of such chains is the focus of future investigations.

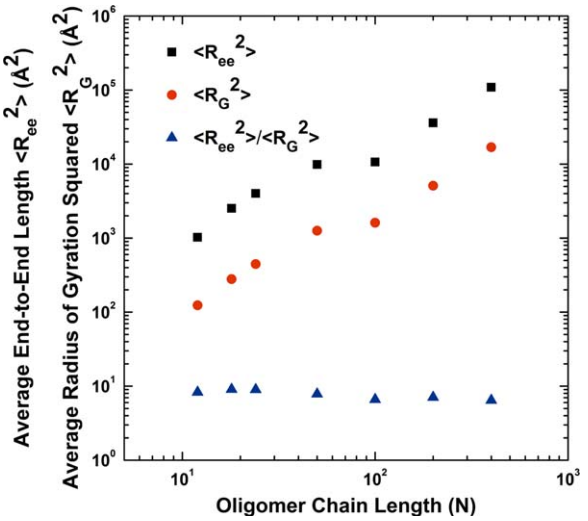

FIGURE 2 $<R_{ee}^2>$ (squares), $<R_G^2>$ (circles), and $<R_{ee}^2>/<R_G^2>$ (triangles) as a function of oligomer chain length (N). [Color figure can be viewed in the online issue, which is available at wileyonlinelibrary.com.]

The value of N_e is based on a modified S-indicator for both kinks and coils.[53] Kinks are defined as segments where the torsion angles are deformed greater than the cutoff angle from a linear chain, and coils are identified when multiple segments of one polymer chain are closer than the cut-off distance to a particular segment of the same or other polymer chain. Modifed S-kink esimators, even when converged and the number of entanglements (<Z>) >> 1, underestimate N_e,[53,55,56] while the modified S-coil estimators (see Fig. 3) overestimate N_e when <Z> is << 1. However, as <Z> increases to >> 1, the entanglement length (via modified S-coil estimators) converges to a realistic value of 60 (N_e) for regioregular P3HT. As the number of monomers in the

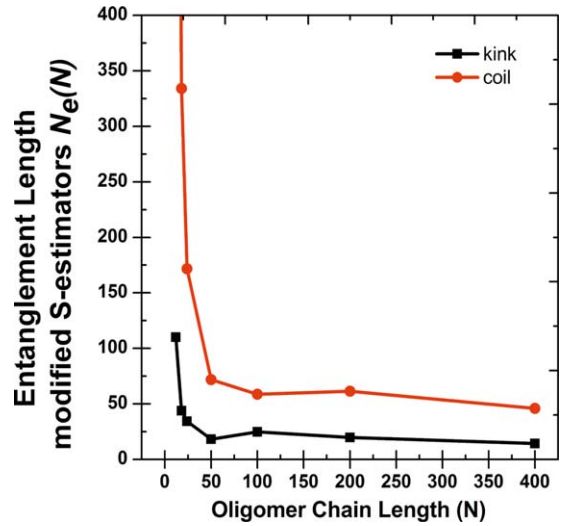

FIGURE 3 Modified S-coil estimators as a function of P3HT chain length. [Color figure can be viewed in the online issue, which is available at wileyonlinelibrary.com.]

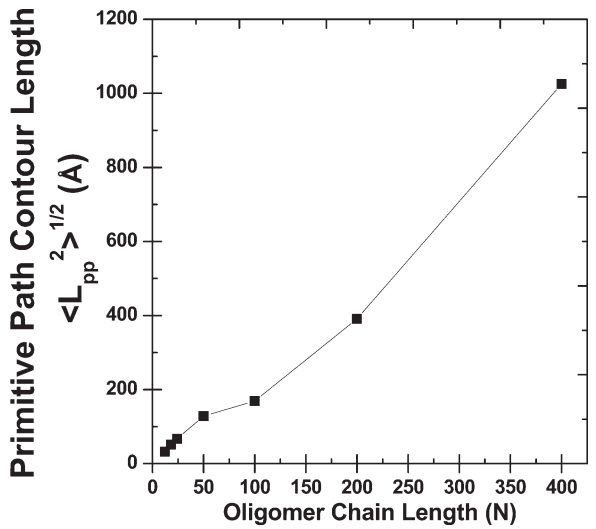

FIGURE 4 Primitive path contour length as computed as a function of oligomer chain length.

oligomer chains increase, the value of N_e oscillates around 60 before reaching 45 for the 400-mer, which is similar to other well-known polymers.[50,57] The results from the ratio $<R_{ee}^2> : <R_G^2>$ and N_e indicate that at high M_w (beyond 200 monomer units in the oligomer) P3HT behaves as a freely jointed polymer, that is, the polymer chain is long enough such that the correlation between chain segements is lost. As already noted, the persistence length of P3HT is 11–12 monomer units and the equivalent effective freely jointed segment length (twice that of the persistence length) are in excellent agreement with the existing report.[58] Interestingly, the P3HT density is higher than that of most other commonly used polymers indicating strong packing; however, the number of coils in the P3HT bulk is lower than that observed to occur for polymers of similar chain length.[59] We note that coiling in P3HT can also impact the electronic and optical processes of P3HT-based materials – for instance, exciton diffusion along a chain is hindered as the electronic couplings between adjacent segments are reduced.[14,60,61]

The primitive path contour length (L_{pp}) is defined as the length of straight line paths overlaid on the contour of polymer chains derived from MD simulations and connected without intersecting the straight (contour) lines of the other segments of same polymer. Information on the primitive paths aid in computing other topological parameters, such as entanglements and persistence lengths.[50] Two distinct slopes are observed when plotting $<L_{pp}>^{1/2}$ *vs.* N, indicating two characteristic lengths for P3HT (Fig. 4). The smaller characteristic length (≈11, when the line connecting points from the 50-mer to the 12-mer is extrapolated to $y = 0$) is the persistence length. The ratio of the end-to-end length to the contour tube length (L_{pp}) is an indication of the rigidity of a polymer chain. Interestingly, this ratio is 1.0 for 12-mer, suggesting that the persistence length for a regioregular P3HT polymer is close to 12. This number is also approximately equal to the number of monomer units required to appropriately describe the electronic and optical properties of P3HT with electronic-structure theories (e.g., 10 to 12 monomers, 3.5 to 4 nm).[21,24,25] This is larger, however, than the persistence length measured experimentally (5 to 7 monomers, 2 to 2.5 nm).[62–64] Recall, however, that persistence length is dependent on solvent conditions and regioregularity.[65] As a point of comparison, the persistence length of polymethylmethacrylate (PMMA), a widely used commercial polymer, is 0.3 nm,[66] which is an order of magnitude smaller than that of P3HT and reveals the comparatively stronger rigidity of the P3HT conjugated backbone. This result is consistent with experiments for poly-(3-butyl thiophene),[67] and recent MD simulation results from using 20-mer 3-hexylthiophene (persistence length of ∼5.0–5.5 nm).[68]

The larger characteristic length (when the line connecting points from the 400-mer to the 100-mer is extrapolated to $y = 0$ in Fig. 4) indicates that $N_e \approx 50$. The ratio of end-to-end length to L_{pp} is ≥ 0.5 (for less than 200-mers) suggesting that even though the polymer length is greater than N_e, P3HT behaves like a semirigid polymer for chain lengths less than 200 monomers and as a freely jointed chain for chains larger than 200 monomers.[54] This reveals that P3HT cohesion should be highly limited due to insignificant entanglements before reaching N_e (i.e., for M_w below ∼10 kDa). The polymer chains, due to the low entanglement density, can easily slide past each other under mechanical deformation when the number of monomers in the polymer chains are less than two-to-four times N_e (10–30 kDa). Interestingly, the onset of the change in exciton coherence and morphology of P3HT films occurs around 20 kDa (125 monomers),[18] approximately two times N_e, indicating that inter-polymer chain entanglements effect the exciton coherence lengths within polymer films.

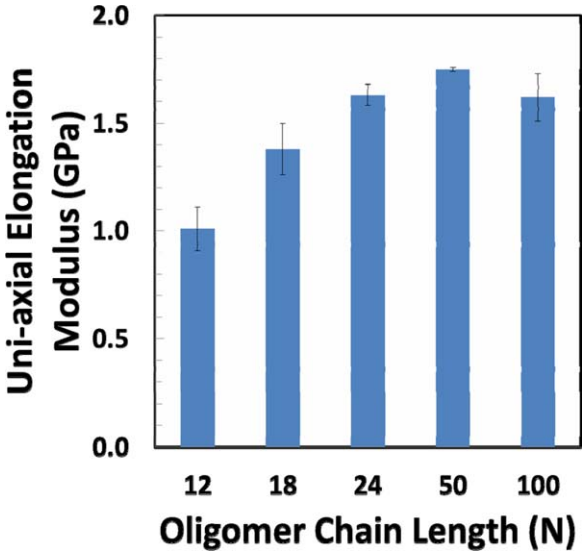

FIGURE 5 Uni-axial elongation modulus as a function of chain length for P3HT. [Color figure can be viewed in the online issue, which is available at wileyonlinelibrary.com.]

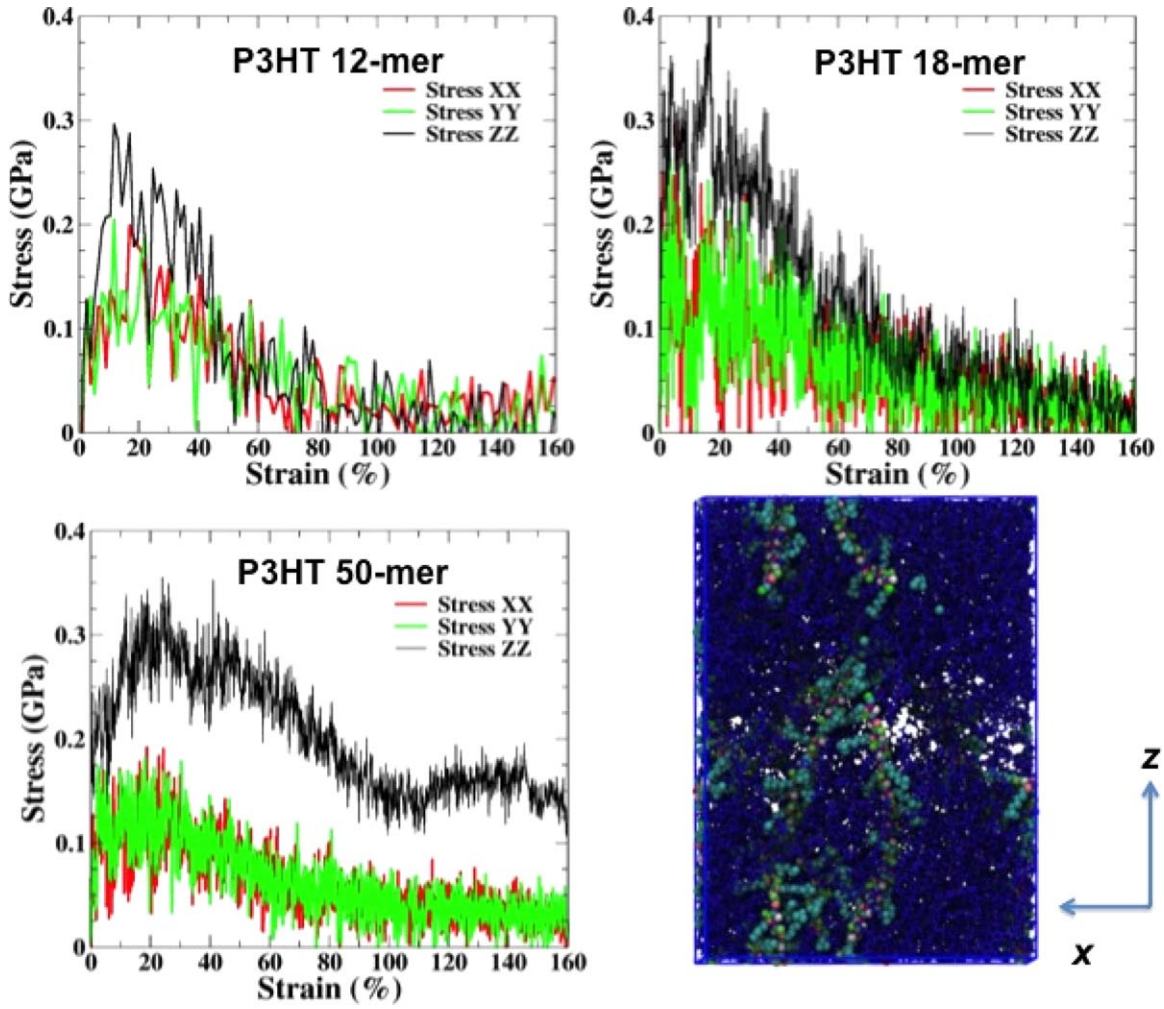

FIGURE 6 Stress response of P3HT with different chain lengths when deformed along *z*-dimension at a strain rate of 0.1 nm/ps. Bottom-right picture depicts the alignment of P3HT (cyan, red colored spheres) molecules along the *z*-direction within the P3HT bulk (blue colored). [Color figure can be viewed in the online issue, which is available at wileyonlinelibrary.com.]

Although we obtain values for N_e and the persistence length, the results from all-atom MD simulations cannot directly quantify the amorphous and crystalline domains in a P3HT layer,[18] due to the necessity of longer timescales for appropriate kinetics. Simulations with oligomers of 15 to 20 monomers are not able to reliably predict the properties of amorphous polymer phases,[19,69] and it appears to be fortuitous that simulations employing short oligomers provide simulated X-ray scattering data for the crystalline phases that coincide with experiment. Large coarse grained simulations,[70] especially with chain lengths greater than N_e and accurate dihedral parameters, are required to demonstrate that such morphological features can be obtained from simulations. This suggests a word of caution concerning the interpretation of phase segregation and polymer:fullerene blend morphologies from simulations that make use of short oligomers.[71]

In the remainder, we focus on the mechanical and deformation behavior of P3HT as a function of M_w. The uni-axial tensile modulus computed for the 12-mer through 100-mer P3HT systems converges to 1.6 GPa (Fig. 5) at a chain length of 100 monomers, in agreement with experiment.[31,34,72] Notably, the plot reveals that simulations of polymer:fullerene mixtures[73] require at minimum 50-mer chains ($\approx N_e$; where the stress vs. strain curve shows a plateau stress). Since the modulus is the stress response in the initially elastic regime, the magnitude of this value does not change significantly as long as the polymer chain length is $\geq N_e$, as observed from the initial results of P3HT with varying chain lengths (Figs. 6 and 7). The accurate description of the uni-axial modulus, N_e, and persistence length points to the fact that the force field employed to describe P3HT is accurate and the results from these simulations can be used reliably to understand experimental results.

The stress response curves upon elongation in the z-direction (Fig. 6) reveal that P3HT shows greater stress along the strain axis compared to the orthogonal directions (marginally when P3HT is modeled with less than 50

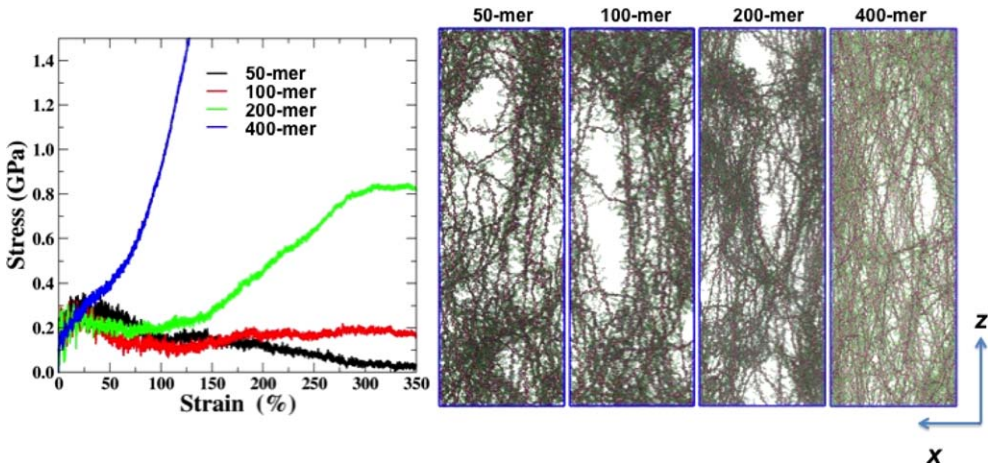

FIGURE 7 Stress response of P3HT with different chain lengths (when <Z> is greater than 1) when deformed along the *z*-direction at a strain rate of 0.1 nm/ps. Representative simulation snapshots of P3HT polymer with varying chain lengths at ≈ 200% strain. Opaque bonds represent the P3HT thiophene backbone and the transparent bonds represent the alkyl side-chains. [Color figure can be viewed in the online issue, which is available at wileyonlinelibrary.com.]

monomers). The magnitude of the initial elastic response is 0.3 GPa for all chain lengths. However at 25% strain, cohesive failure results when chain lengths are smaller than 50 monomers. Only when chains of 50 monomers or larger are used is a plateau (yielding) stress observed. Polymer chains under tension slide past each other causing frictional resistance, which is indicative of entangled polymers and fibril formation. A snapshot of fibril formation at a strain of 25% is shown in the lower right panel of Figure 6. In addition, an increase in the flow stress (at > 100% strain, stress required by the polymer to expand at the given rate) is observed with increasing chain length (see Fig. 7). Depending on the temperature, the ratio of the maximum stress to the plateau stress converges at 3 to 5 for either flexible or semiflexible polymers with $N/N_e \geq 8$.[74] A ratio of 4 is observed for P3HT with 200 monomers, but for larger polymers the stress response is primarily due to the tensile stress in the bonds and, hence, the high stress values obtained for the 400-mer system may be unrealistic [due to the use of the harmonic bond approximation rather than the finite extensible nonlinear elasticity (FENE) model]. Representative snapshots for 50-mer through 400-mer at 200% strain are shown in Figure 7. The noticeable presence of large voids within the simulation box diminishes with increasing P3HT M_w, and we observe more uniformly stretched polymer backbones (opaque bonds) due to increased entanglements within the polymer network.

Uniform elongation of polymer segments in a thin film is an indication of consistent entanglements within the cross sectional area. The cohesion energy is a function of the number of entanglements per unit cross sectional area, since significant contribution to the cohesion energy is due to plastic deformation (mostly of the polymer) of the bulk heterojunction (BHJ) layer around the crack tip, which dissipates much of the applied mechanical strain energy.[24] The fracture (cohesion) energy of a BHJ layer consisting of P3HT ($M_w < 53$ kDa, 340 thiophene units) and a substituted fullerene is measured to be 2.5 J/m^2,[2,23] and the fracture energy increases with the increase in the polymer M_w.[24] Increased cohesion indicates a larger number of entanglements near the crack tip for P3HT M_w larger than 50 kDa (an increase in cohesion with the increase in active layer thickness that is akin to crosslinked polymers). This particular result is of interest as at $M_w \approx 50$ kDa there is a noted change in the exciton spatial distribution of P3HT, suggesting an association between the mechanical and electronic characteristics.[18]

The simulations suggest that P3HT with chain lengths of 200 monomers or more can possess truly significant degrees of entanglement. However, a chain length of 200 is smaller than that determined experimentally (around 50 kDa [300 monomers]) for the transition to either high cohesive strength[24] or entangled regions.[18] Part of the complexitiy with P3HT arises from its semicrystalline nature, since P3HT has no entanglements within the crystalline domains. Hence, 200-monomer P3HT should be considered a lower bound to observe both crystalline and amorphous regions. For polymer:fullerene BHJ, these results suggest that the amorphous regions of the pure polymer phase should be large so as to provide significant entanglement density to enhance fracture resistance. Notably, the addition of fullerenes to the polymer decreases the number of entanglements,[73] and therefore even larger M_w may be required for large cohesion in BHJ active layers. The simulations presented here suggest that P3HT films with good mechanical properties should occur for chain lengths greater than 200 monomers ($M_w > 35$ kDa). The dynamics of pure regioregular melt and mixtures of regio and random P3HT will be the focus of future studies.

CONCLUSIONS

In conclusion, MD simulations were employed to study the polymeric and mechanical properties of P3HT with varying

M_w. The persistence length was shown to be 10 to 12 monomers, which compares well with the observed polaron delocalization lengths. The computed entanglement length of P3HT is approximately 50 to 60 monomers, which is validated from multiple criteria; however, P3HT does not strongly entangle until much larger M_w values (at least 200 monomers or 35 kDa) are considered.

By modeling the stress–strain response for P3HT, the uniaxial tensile modulus was determined and the tensile stress was shown to increase and converge for P3HT oligomers of at least 100 monomers. Our results also suggest that for regioregular monodisperse P3HT to resist deformation and have high fracture energies, the M_w needs to be greater than 35 kDA. More importantly, the simulations reveal that very long oligomer chains are required to accurately model the amorphous and entangled regions in P3HT. This result is critical not only for studying the mechanical properties but also for accurately modeling the charge–carrier transport properties since these can be can only be reliably described for amorphous thin films in the limit of sufficient entanglements. To understand the fate of a charge moving from a crystalline to an amorphous segment within a bulk polymer would require polymer chain lengths to be much larger than N_e.

The results presented here are useful in the context of the numerous studies evaluating the mechanical stability and reliability of (opto)electronic active layers. Simulations can aid in the determination of polymer M_w requirements for device applications. However, it cannot be stressed strongly enough that extreme care must be taken in the theoretical determination of these properties owing to the wide variety of chemistries currently in use and limited force-field parameters for π-conjugated molecules and polymers.

ACKNOWLEDGMENTS

The authors gratefully acknowledge financial support of this work in part by the Center for Advanced Molecular Photovoltaics (CAMP, Award KUS-C1-015-21) made possible by the King Abdullah University of Science and Technology (KAUST) and by the Office of Naval Research (Award No. N00014-14-1-0171); computing resources were provided through the Chemistry Research Instrumentation and Facilities (CRIF) Program, Award Number CHE-0946869, and the Oklahoma Super Computing Center for Education and Research (OSCER). The authors thank Professor Martin Kröger (ETH Zürich) for the Z1 software package.

REFERENCES AND NOTES

1 H. Shirakawa, E. J. Louis, A. G. MacDiarmid, C. K. Chiang, A. J. Heeger, *J. Chem. Soc. Chem. Commun.* **1977**, *16*, 578–580.

2 S. Bauer, S. Bauer-Gogonea, I. Graz, M. Kaltenbrunner, C. Keplinger, R. Schwödiauer, *Adv. Mater.* **2014**, *26*, 149–162.

3 B. Adhikari, S. Majumdar, *Prog. Polym. Sci.* **2004**, *29*, 699–766.

4 Applications of Organic and Printed Electronics, 1 ed.; Springer US, **2013**. Editor: Cantatore, Eugenio.

5 T.-A. Chen, X. Wu, R. D. Rieke, *J. Am. Chem. Soc.* **1995**, *117*, 233–244.

6 K. M. Coakley, M. D. McGehee, *Chem. Mater.* **2004**, *16*, 4533–4542.

7 A. Marrocchi, D. Lanari, A. Facchetti, L. Vaccaro, *Energy Environ. Sci.* **2012**, *5*, 8457–8474.

8 K. N. Schwarz, T. W. Kee, D. M. Huang, *Nanoscale* **2013**, *5*, 2017–2027.

9 Y. Y. Yimer, A. Dhinojwala, M. Tsige, *J. Chem. Phys.* **2012**, *137*, 044703.

10 R. S. Bhatta, Y. Y. Yimer, D. S. Perry, M. Tsige, *J. Phys. Chem. B* **2013**, *117*, 10035–10045.

11 K. Do, D. M. Huang, R. Faller, A. J. Moule, *Phys. Chem. Chem. Phys.* **2010**, *12*, 14735–14739.

12 F. P. V. Koch, M. Heeney, P. Smith, *J. Am. Chem. Soc.* **2013**, *135*, 13699–13709.

13 M. Koppe, C. J. Brabec, S. Heiml, A. Schausberger, W. Duffy, M. Heeney, I. McCulloch, *Macromolecules* **2009**, *42*, 4661–4666.

14 T. Adachi, J. Brazard, R. J. Ono, B. Hanson, M. C. Traub, Z.-Q. Wu, Z. Li, J. C. Bolinger, V. Ganesan, C. W. Bielawski, D. A. Vanden Bout, P. F. Barbara, *J. Phys. Chem. Lett.* **2011**, *2*, 1400–1404.

15 P. Kohn, S. Huettner, H. Komber, V. Senkovskyy, R. Tkachov, A. Kiriy, R. H. Friend, U. Steiner, W. T. S. Huck, J.-U. Sommer, M. Sommer, *J. Am. Chem. Soc.* **2012**, *134*, 4790–4805.

16 A. M. Ballantyne, L. Chen, J. Dane, T. Hammant, F. M. Braun, M. Heeney, W. Duffy, I. McCulloch, D. D. C. Bradley, J. Nelson, *Adv. Funct. Mater.* **2008**, *18*, 2373–2380.

17 C. Scharsich, R. H. Lohwasser, M. Sommer, U. Asawapirom, U. Scherf, M. Thelakkat, D. Neher, A. Köhler, *J. Polym. Sci. Part B: Polym. Phys.* **2012**, *50*, 442–453.

18 F. Paquin, H. Yamagata, N. J. Hestand, M. Sakowicz, N. Bérubé, M. Côté, L. X. Reynolds, S. A. Haque, N. Stingelin, F. C. Spano, C. Silva, *Phys. Rev. B: Condens. Matter* **2013**, *88*, 155202.

19 F. P. V. Koch, J. Rivnay, S. Foster, C. Müller, J. M. Downing, E. Buchaca-Domingo, P. Westacott, L. Yu, M. Yuan, M. Baklar, Z. Fei, C. Luscombe, M. A. McLachlan, M. Heeney, G. Rumbles, C. Silva, A. Salleo, J. Nelson, P. Smith, N. Stingelin, *Prog. Polym. Sci.* **2013**, *38*, 1978–1989.

20 J. Peet, J. Y. Kim, N. E. Coates, W. L. Ma, D. Moses, A. J. Heeger, G. C. Bazan, *Nat. Mater.* **2007**, *6*, 497–500.

21 S. B. Darling, M. Sternberg, *J. Phys. Chem. B* **2009**, *113*, 6215–6218.

22 .Alkyl side chains should be taken into account to get accurate torsional potentials between thiophene units in a polymer.

23 V. Brand, C. Bruner, R. H. Dauskardt, *Sol. Energy Mater. Sol. Cells* **2012**, *99*, 182–189.

24 C. Bruner, R. Dauskardt, *Macromolecules* **2014**, *47*, 1117–1121.

25 C. Bruner, N. C. Miller, M. D. McGehee, R. H. Dauskardt, *Adv. Funct. Mater.* **2013**, *23*, 2863–2871.

26 S. R. Dupont, M. Oliver, F. C. Krebs, R. H. Dauskardt, *Sol. Energy Mater. Sol. Cells* **2012**, *97*, 171–175.

27 D. J. Lipomi, B. C. K. Tee, M. Vosgueritchian, Z. Bao, *Adv. Mater.* **2011**, *23*, 1771–1775.

28 T. F. O'Connor, A. V. Zaretski, B. A. Shiravi, S. Savagatrup, A. D. Printz, M. I. Diaz, D. J. Lipomi, *Energy Environ. Sci.* **2014**, *7*, 370–378.

29 S. Savagatrup, A. S. Makaram, D. J. Burke, D. J. Lipomi, *Adv. Funct. Mater.* **2014**, *24*, 1169–1181.

30 A. Gasperini, K. Sivula, *Macromolecules* **2013**, *46*, 9349–9358.

31 B. O'Connor, E. P. Chan, C. Chan, B. R. Conrad, L. J. Richter, R. J. Kline, M. Heeney, I. McCulloch, C. L. Soles, D. M. DeLongchamp, *ACS Nano* **2010**, *4*, 7538–7544.

32 O. Awartani, B. I. Lemanski, H. W. Ro, L. J. Richter, D. M. DeLongchamp, B. T. O'Connor, *Adv. Energy Mater.* **2013**, *3*, 399–406.

33 A. J. Baca, J.-H. Ahn, Y. Sun, M. A. Meitl, E. Menard, H.-S. Kim, W. M. Choi, D.-H. Kim, Y. Huang, J. A. Rogers, *Angew. Chem. Int. Ed.* **2008**, *47*, 5524–5542.

34 D.-Y. Khang, J. A. Rogers, H. H. Lee, *Adv. Funct. Mater.* **2009**, *19*, 1526–1536.

35 P. Steve, *J.Comput. Phys.* **1995**, *117*, 1–19.

36 W. L. Jorgensen, D. S. Maxwell, J. Tirado-Rives, *J. Am. Chem. Soc.* **1996**, *118*, 11225–11236.

37 D. M. Huang, R. Faller, K. Do, A. J. Moulé, *J. Chem. Theory Comput.* **2009**, *6*, 526–537.

38 S. Nose, *J. Chem. Phys.* **1984**, *81*, 511–519.

39 M. E. Tuckerman, J. Alejandre, R. López-Rendón, A. L. Jochim, G. J. Martyna, *J. Phys. A: Math. Gen.* **2006**, *39*, 5629.

40 J. Zhao, A. Swinnen, G. Van Assche, J. Manca, D. Vanderzande, B. V. Mele, *J. Phys. Chem. B* **2009**, *113*, 1587–1591.

41 P. E. Hopkinson, P. A. Staniec, A. J. Pearson, A. D. F. Dunbar, T. Wang, A. J. Ryan, R. A. L. Jones, D. G. Lidzey, A. M. Donald, *Macromolecules* **2011**, *44*, 2908–2917.

42 M. E. Tuckerman, C. J. Mundy, S. Balasubramanian, M. L. Klein, *J. Chem. Phys.* **1997**, *106*, 5615–5621.

43 D. Frenkel, B. Smit, Understanding Molecular Simulation: From Algorithms to Applications, 2nd ed.; Academic Publishers: London, **2002**.

44 J. Mårdalen, E. J. Samuelsen, O. R. Gautun, P. H. Carlsen, *Solid State Commun.* **1991**, *77*, 337–339.

45 T. J. Prosa, M. J. Winokur, J. Moulton, P. Smith, A. J. Heeger, *Macromolecules* **1992**, *25*, 4364–4372.

46 S. Rane, P. D. Gujrati, *Phys. Rev. E* **2001**, *64*, 011801.

47 S. S. Jawalkar, K. V. S. N. Raju, S. B. Halligudi, M. Sairam, T. M. Aminabhavi, *J. Phys. Chem. B* **2007**, *111*, 2431–2439.

48 M. M. Francl, W. J. Petro, W. J. Hehre, J. S. Binkley, M. S. Gordon, D. J. DeFrees, J. A. Pople, *J. Chem. Phys.* **1982**, *77*, 3654.

49 F. Machui, S. Abbott, D. Waller, M. Koppe, C. J. Brabec, *Macromol. Chem. Phys.* **2011**, *212*, 2159–2165.

50 K. Foteinopoulou, N. C. Karayiannis, V. G. Mavrantzas, M. Kröger, *Macromolecules* **2006**, *39*, 4207–4216.

51 S. Shanbhag, M. Kröger, *Macromolecules* **2007**, *40*, 2897–2903.

52 N. C. Karayiannis, M. Kröger, *Int. J. Mol. Sci.* **2009**, *10*, 5054–5089.

53 R. S. Hoy, K. Foteinopoulou, M. Kröger, *Phys. Rev. E* **2009**, *80*, 031803.

54 M. Doi, Introduction to Polymer Physics; Oxford University Press, London, UK **1996**.

55 P. J. Flory, Statistical Mechanics of Chain Molecules, Repr. ed. with corrections/ed.; Munich: Hanser Publishers, **1989**.

56 J. A. S. Rudi, T. Christos, L. Ying, L. Wing Kam, K. Martin, D. S. Jay, *N. J. Phys.* **2014**, *16*, 015027.

57 A. G. Mikos, N. A. Peppas, *J. Chem. Phys.* **1988**, *88*, 1337–1342.

58 J.-M. Y. Carrillo, R. Kumar, M. Goswami, B. G. Sumpter, W. M. Brown, *Phys. Chem. Chem. Phys.* **2013**, *15*, 17873–17882.

59 L. J. Fetters, D. J. Lohse, D. Richter, T. A. Witten, A. Zirkel, *Macromolecules* **1994**, *27*, 4639–4647.

60 E. Collini, G. D. Scholes, *Science* **2009**, *323*, 369–373.

61 D. Beljonne, G. Pourtois, C. Silva, E. Hennebicq, L. M. Herz, R. H. Friend, G. D. Scholes, S. Setayesh, K. Müllen, J. L. Brédas, *Proc. Natl. Acad. Sci. USA* **2002**, *99*, 10982–10987.

62 G. W. Heffner, D. S. Pearson, *Macromolecules* **1991**, *24*, 6295–6299.

63 J. Niklas, K. L. Mardis, B. P. Banks, G. M. Grooms, A. Sperlich, V. Dyakonov, S. Beaupre, M. Leclerc, T. Xu, L. Yu, O. G. Poluektov, *Phys. Chem. Chem. Phys.* **2013**, *15*, 9562–9574.

64 J.-F. Chang, J. Clark, N. Zhao, H. Sirringhaus, D. W. Breiby, J. W. Andreasen, M. M. Nielsen, M. Giles, M. Heeney, I. McCulloch, *Phys. Rev. B: Condens. Matter* **2006**, *74*, 115318.

65 P. K. Choudhury, D. Bagchi, C. S. S. Sangeeth, R. Menon, *J. Mater. Chem.* **2011**, *21*, 1607–1614.

66 C. Ortiz, G. Hadziioannou, *Macromolecules* **1999**, *32*, 780–787.

67 J. P. Aime, F. Bargain, M. Schott, H. Eckhardt, G. G. Miller, R. L. Elsenbaumer, *Phys. Rev. Lett.* **1989**, *62*, 55–58.

68 O. Alexiadis, V. G. Mavrantzas, *Macromolecules* **2013**, *46*, 2450–2467.

69 J. Rivnay, S. C. B. Mannsfeld, C. E. Miller, A. Salleo, M. F. Toney, *Chem. Rev.* **2012**, *112*, 5488–5519.

70 R. Kumar, M. Goswami, B. G. Sumpter, V. N. Novikov, A. P. Sokolov, *Phys. Chem. Chem. Phys.* **2013**, *15*, 4604–4609.

71 H. S. Marsh, A. Jayaraman, *J. Polym. Sci. Part B: Polym. Phys.* **2013**, *51*, 64–77.

72 D. Tahk, H. H. Lee, D.-Y. Khang, *Macromolecules* **2009**, *42*, 7079–7083.

73 N. R. Tummala, C. Bruner, C. Risko, J.-L. Bredas, R. H. Dauskardt, submitted for publication.

74 J. Rottler, S. Barsky, M. O. Robbins, *Phys. Rev. Lett.* **2002**, *89*, 148304.